The Astrophysical Journal, 904:57 (7pp), 2020 November 20 https://doi.org/10.3847/1538-4357/abbd99

Two Candidate High-redshift X-Ray Jets without Coincident Radio Jets

D. A. Schwartz[1], A. Siemiginowska[1], B. Snios[1], D. M. Worrall[2], M. Birkinshaw[2], C. C. Cheung[3], H. Marshall[4], G. Migliori[5], J. F. C. Wardle[6], and Doug Gobeille[7]
[1] Smithsonian Astrophysical Observatory, Cambridge, MA 02138, USA; dschwartz@cfa.harvard.edu
[2] HH Wills Physics Laboratory, University of Bristol, Tyndall Avenue, Bristol BS8 1TL, UK
[3] Space Science Division, Naval Research Laboratory, Washington, DC 20375-5352, USA
[4] Kavli Institute for Astrophysics and Space Research, Massachusetts Institute of Technology, 77 Massachusetts Avenue, Cambridge, MA 02139, USA
[5] INAF Istituto di Radioastronomia, via Gobetti 101, I-40129 Bologna, Italy
[6] Department of Physics, MS 057, Brandeis University, Waltham, MA 02454, USA
[7] Department of Physics, University of Rhode Island, 45 Upper College Road, Kingston, RI 02881, USA
Received 2020 July 27; revised 2020 September 14; accepted 2020 September 29; published 2020 November 20

Abstract

We report the detection of extended X-ray emission from two high-redshift radio quasars. These quasars, J1405+0415 at $z = 3.208$ and J1610+1811 at $z = 3.118$, were observed in a Chandra snapshot survey selected from a complete sample of the radio-brightest quasars in the overlap area of the VLA-FIRST radio survey and the Sloan Digital Sky Survey. The extended X-ray emission is located along the line connecting the core to a radio knot or hotspot, favoring the interpretation of X-ray jets. The inferred rest-frame jet X-ray luminosities from 2 to 30 keV would be of order 10^{45} erg s^{-1} if emitted isotropically and without relativistic beaming. In the scenario of inverse Compton scattering of the cosmic microwave background (CMB), X-ray jets without a coincident radio counterpart may be common, and should be readily detectable to redshifts even beyond 3.2 due to the $(1+z)^4$ increase of the CMB energy density compensating for the $(1+z)^{-4}$ cosmological diminution of surface brightness. If these can be X-ray confirmed, they would be the second and third examples of quasar X-ray jets without detection of underlying continuous radio jets.

Unified Astronomy Thesaurus concepts: Non-thermal radiation sources (1119); Galaxy jets (601); Radio loud quasars (1349); X-ray quasars (1821); X-ray active galactic nuclei (2035)

1. Introduction

Although the first jet from an active galactic nuclei was discovered as a visible image in a photograph of M87 (Curtis 1918), they have been observed primarily as radio phenomena (e.g., Turland 1975; Waggett et al. 1977; Readhead et al. 1978; Perley et al. 1979; Bridle & Perley 1984). Jets provide a mechanism to explain the morphologies of extragalactic radio sources and to supply the large energy content inferred in lobes of extragalactic radio sources (e.g., Rees 1971; Longair et al. 1973; Blandford & Rees 1974; Scheuer 1974). Jets transport energy from the central supermassive black hole to radio lobes, doing work on the external medium, and playing a significant role in the energy budget of black hole accretion. It is now recognized that extragalactic jets play an essential role in the feedback processes that prevent catastrophic cooling-flow collapse in clusters of galaxies (e.g., Fabian et al. 2000; Fabian 2012; Hardcastle & Croston 2020).

Multiwavelength data are important for understanding the physics of these systems. The Chandra X-ray Observatory has enabled X-ray observations to contribute significantly to the study of the power and morphology of jets in extragalactic sources (Harris & Krawczynski 2006; Worrall 2009; Schwartz 2010). Using a model-dependent assumption that the X-rays are generated by inverse Compton (IC) up-scattering of the cosmic microwave background (CMB) radiation (Tavecchio et al. 2000; Celotti et al. 2001), X-rays help estimate the enthalpy flux, often simply called "power," that does work on the external medium resulting in feedback. The power carried by kiloparsec-scale jets has generally been estimated by assessment of the energy deposited into radio lobes and cocoons (Scheuer 1974; Rawlings & Saunders 1991; Willott et al. 1999), or by the energy required to create cavities observed in the hot intracluster or intragalactic gas at low redshift (Bîrzan et al. 2008), or by empirical scaling relations derived from those methods (e.g., O'Dea et al. 2009; Cavagnolo et al. 2010; Daly et al. 2012). Those are all based on calorimetry coupled with an estimate of age to give an average power output. The IC/CMB interpretation of the X-ray observations offers an alternative method of estimating power by measurements of the jet itself.

At high redshift, several factors favor jets manifesting as X-ray via IC/CMB rather than as radio emitters. The radio surface brightness suffers the cosmological diminution factor $(1+z)^{-4}$, while for IC/CMB X-ray emission this is compensated by the $(1+z)^4$ increase in the CMB energy density. Another factor is the ≈100 times longer lifetimes of the electrons with energies of order 100 MeV producing X-rays via IC/CMB, compared to the electrons with order of 10 GeV that give the GHz synchrotron radiation. In addition, the observed radio emission is more diminished by the redshift than the X-rays since the radio spectrum tends to steepen at emitted mm-wave frequencies, while the X-rays generally have a flatter spectrum. However, searching for new examples of relativistic kpc-scale X-ray jets with Chandra, the only current instrument capable of detecting them, is observationally expensive as only those few percent of radio quasars that are beamed tightly in our direction are viable candidate systems. The vast majority of X-ray jet detections therefore result from pointed observations of known radio jets.

Serendipitously, Simionescu et al. (2016) discovered the first, dramatic example of an X-ray jet resolved on arcsecond scale and without a corresponding radio jet detection. Here we present two further candidates, the quasars J1405+0415 at $z = 3.208$ (Barthel et al. 1990), and J1610+1811 at $z = 3.118$ (Osmer et al. 1994).[8] These systems are distinguished by the absence of a detectable radio jet. Preliminary results have been presented in Schwartz et al. (2019).

We adopt $H_0 = 67.8$ km s^{-1} Mpc^{-1}, $\Omega_M = 0.308$, and $\Omega_\Lambda = 0.692$, (Planck Collaboration et al. 2016), giving scales of 7.8 and 7.7 kpc arcsec^{-1} for redshifts of 3.1 and 3.2, respectively. We use the terminology definitions of Bridle et al. (1994) to describe the radio features. Spectral indices α are defined by flux density $S_\nu \propto \nu^{-\alpha}$. Photon number indices are $\alpha + 1$, and corresponding relativistic electron number spectra are $dN/d\gamma \propto \gamma^{-(2\alpha+1)}$, where γ is the electron Lorentz factor.

2. The High-redshift Sample

We carried out an exploratory survey for X-ray jets associated with high-redshift radio-loud quasars. Our sample was drawn from the complete survey of Gobeille (2011) and Gobeille et al. (2014). That survey included the 123 radio-brightest quasars at redshifts greater than 2.5 in the overlapping region of the VLA-FIRST radio survey (Becker et al. 1995) and the Sloan Digital Sky Survey (Abazajian et al. 2003). The quasars were selected to have a total flux density >70 mJy at either 1.4 or 5 GHz, and required to have a spectroscopically measured redshift. In that sample, 61 systems show resolved radio structure detected with 1″ or finer resolution, and from these we eliminated 30 that were classified as triples since they are not likely to be relativistically beamed in our direction as is necessary to reveal IC/CMB emission. This left 31 sources with resolved radio structure, for which we ignored morphological distinctions such as jet, knot, hotspot, or lobe. We took the 16 with redshifts $z > 3$ as most likely to be detected in short, 10 ks Chandra "snapshot" observations to look for jets suitable for further follow-up observations. Of these 16, we did not re-observe two quasars previously detected, J1430+4204 (Cheung et al. 2012) at $z = 4.7$, and J1510+5702 (Siemiginowska et al. 2003; Yuan et al. 2003) at $z = 4.3$. Each quasar has one well-defined direction given by an extended radio feature.

This paper presents two cases of extended X-ray emission without co-spatial radio emission. A posteriori the extended emissions are just at the 99.7% confidence limit, giving a 0.17% chance that such a result could arise in 14 trials, and a 4.2% chance of one such false detection. For comparison, a 99% confidence result would have allowed a 13% chance of one such false positive in 14 trials. In the survey of 14 objects we have significant X-ray emission external to the quasar core in five of the sources, including the two reported here, as will be reported by B. Snios et al. (2020, in preparation), along with the quasar core data.

The survey observations were done with Advanced CCD Imaging Spectrometer (ACIS) S-3, in the standard 1/4 subarray timed exposure mode, with very faint telemetry format. Pile-up was less than 2.5% for each quasar, and was neglected in the analysis. In the 0.5–7.0 keV X-ray band, background from the diffuse X-ray sky and from non-X-ray events was very small; 0.0273 ± 0.0027 counts arcsec^{-2} for J1405, and 0.0195 ± 0.0011 counts arcsec^{-2} for J1610. Therefore we only used the standard faint mode telemetry processing for reconstructing each individual photon event. All observations had a roll direction preference such that the extended radio feature would not coincide with the ACIS readout streak. Each observation was approved for 10 ks on target, which would result in a nominal 9.6 ks live time after correction for the 4.88% dead-time due to the 1/4 subarray readout. Chandra observed J1405 (ObsID 20408) for 9.6 ks live time on 2018 May 8, and J1610 (ObsID 20410) for 9.1 ks live time on 2018 May 24. We used CIAO software version 4.12 (Fruscione et al. 2006) and CALDB version 4.9 in data analysis.

To compare with the X-ray images, we obtained new Karl G. Jansky Very Large Array (VLA) A-array data (program 12B-230). A total of 5.3 minutes of exposure was obtained for each source on 2012 November 18 (J1405) and 2012 December 8 (J1610). The data were calibrated and imaged with CASA using standard procedures. Each data set used two intermediate-frequency bands (1 GHz bandwidth each) centered at 4.9 and 7.4 GHz, giving an effective center frequency of the resultant images at 6.2 GHz.

3. Extended X-Ray Emission

The identification as X-ray jets can be justified by the fact that we have a statistically significant detection of X-ray photons in an extended linear region defined by the direction of the central source to radio emission in an external knot or hotspot. The region width is defined by the Chandra spatial resolution. The existence of an external radio feature means it must have been, or currently is being, powered by a jet. Because of our limited statistics, we cannot claim we have detected extended X-ray jets according to the formal definition of having a length at least four times its width (Bridle & Perley 1984).

The dominant background for detecting an arcsec-scale jet is scattered X-rays from the quasar nucleus. For each object, we fit a power-law spectrum to the quasar. We use that spectrum in saotrace-2.0.4_03[9] to generate rays which are passed to marx-5.5.0[10] (Davis et al. 2012) to simulate an ACIS-S image. We use Marx with the energy dependent sub-pixel event redistribution (EDSER) algorithm. We run 500 separate simulations with the actual source flux, observing time, and aspect dithering, in order to accurately simulate the pile-up and the ACIS readout streak. The resulting files are merged into a single, simulated image of the point-spread function. The simulated image counts are normalized by the ratio of counts in a 0.″95 radius about the quasar, compared to counts in the same region of the simulated image. The error in this normalization is dominated by the number of counts observed from the quasar, and in turn determines the uncertainty in the expected number of scattered X-rays in the jet region. The 0.″95 radius contains a nominal 90% encircled counts at 1.5 keV, but for the broad quasar spectral distribution our simulations give 83.6% and 83.7% respectively for J1405 and J1610. This 0.″95 radius is an objective choice of a distance to search for emission external to the quasar core, and is used for J1405. However, since quasar J1610 is 40% brighter than J1405, using that same distance criterion would mean that our detection sensitivity threshold

[8] We will refer to these as J1405 and J1610, respectively.

[9] http://cxc.harvard.edu/cal/Hrma/SAOTrace.html

[10] https://space.mit.edu/CXC/MARX/

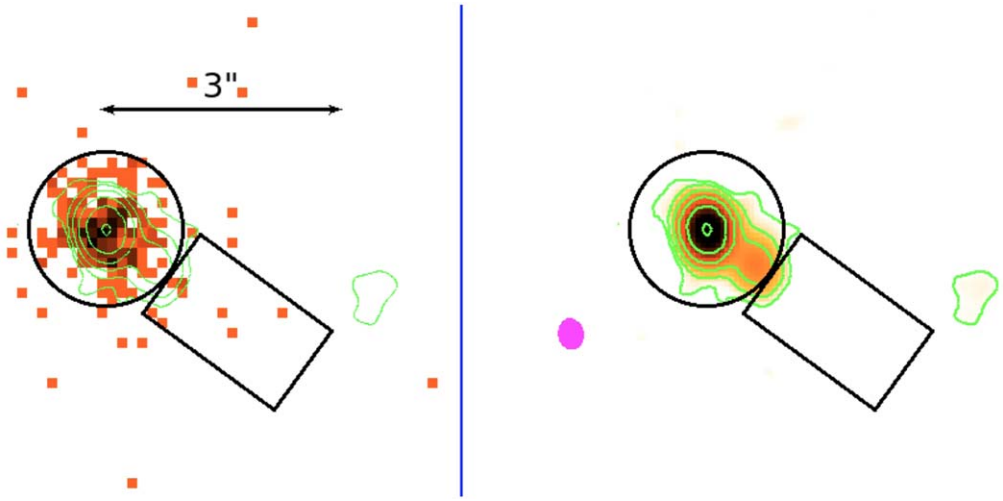

Figure 1. Quasar J1405. Left: 0.5–7.0 keV X-ray data in 0.″123 pixels. Maximum counts are 13 per pixel. Both panels show a 0.″95 radius circle about the quasar and the 2.″0 × 1.″5 box used for the extended region we designate as the jet. Right: our 6.2 GHz VLA data, showing the quasar core, a radio knot at 0.″73 from the quasar at position angle 235°, and a faint hotspot about 3″ away at position angle 257°. Radio contours are shown in both panels, with the lowest level at 0.6 mJy beam^{-1} and increasing by factors of 4, with a peak flux density of 694 mJy beam^{-1}. The restoring beam shown in magenta is 0.″39 × 0.″32 FWHM at 7.°5 position angle.

would be 1.5 times larger. Via simulation we find that for a jet box 1.″3 from J1610, the background due to scattered quasar counts is the same for both objects.

3.1. J1405+0415

The flat spectrum radio source PKS 1402+044 (Shimmins et al. 1975) was identified as a quasi-stellar object by Condon et al. (1977), with a redshift $z = 3.20$ measured by Peterson et al. (1978). VLBI observations showed that a quasar jet was relativistically beamed in our direction on pc scales with components at a range of position angles (measured positive east of north) from 258° to 318° at distances 4.4–14.5 mas from the brightest flux density position (Gurvits et al. 1992). Gurvits et al. (1992) pointed out that these features could be interpreted as a continuous jet, bending through an apparent angle of ≈90° and then pointing toward a knot about 0.″8 away at 237° position angle, and possibly connecting to faint extended emission 3.″3 away at position angle 254°. They concluded that the variation of position angles was most likely due to a jet closely aligned to our line of sight and deflected through a relatively small angle. Higher resolution VLA, Very Long Baseline Array (VLBA), and VLBI Space Observatory Programme (VSOP) multiwavelength observations in 1998 March, and 2004 January and October by Yang et al. (2008) confirmed the morphological structure and resolved further pc-scale components with a range of position angles 232.°2–334.°4. They determined that several of the core components had brightness temperatures near and above 10^{12} K, indicating relativistic motion. For the innermost components they deduced a Doppler factor $\delta > 23$, and an upper limit to the angle to our line of sight of 1°. They fit the GHz spectra of the VLA-observed arcsecond-scale features to power-laws. Renormalizing to our central frequency, they report $670(\nu/6.2_{\rm GHz})^{-0.09}$ mJy for the core, $34(\nu/6.2_{\rm GHz})^{-0.91}$ mJy for the knot, and $2.9(\nu/6.2_{\rm GHz})^{-1.66}$ mJy for the lobe in the 1.4–15.9 GHz range, all in agreement with our measurements as reported below.

Using the Einstein Observatory, Zamorani et al. (1981) first detected X-rays from the quasar, reporting a flux of $(0.8 \pm 0.4) \times 10^{-13}$ erg cm^{-2} s^{-1} in the 0.5–4.5 keV band. Brinkmann et al. (1997) reported a flux of $(2 \pm 1.2) \times 10^{-13}$ erg cm^{-2} s^{-1} in the 0.1–2.4 keV band, based on pointed ROSAT observations. Considering the uncertainties and the bandwidth differences the X-ray flux may have been constant. Both those telescopes had ≈5″ resolution and therefore could not have resolved any small-scale extent.

Figure 1 shows our 0.5–7.0 keV X-ray and 6.2 GHz radio data for J1405. We shifted the Chandra image by 0.″57 so that the quasar centroid coincided with the radio position at $14^{\rm h}05^{\rm m}01.^{\rm s}12$ +4°15′35.″8. We take the quasar region counts inside a 0.″95 radius to determine the X-ray spectrum. The 264 quasar counts are fit to a power law with fixed $n_{\rm H} = 2.19 \times 10^{20}$ H-atoms cm^{-2}, using the Cash statistic in CIAO 4.12 Sherpa version 1 (Freeman et al. 2001). The best fit gives a spectral index $\alpha = 0.38 \pm 0.12$, for which the incident 0.5–7.0 keV flux corrected for Galactic absorption is $(4.0 \pm 0.4) \times 10^{-13}$ erg cm^{-2} s^{-1}, corresponding to a rest-frame luminosity of $(3.8 \pm 0.4) \times 10^{46}$ erg s^{-1} in the 2.1–29.4 keV band. The flux is consistent with the ROSAT flux, but a factor of two higher than that measured with Einstein, all extrapolated to the same energy range.

The rectangle in Figure 1 shows the region we take for the X-ray jet. It is extended 2″ beyond the quasar region, parallel to and straddling the line from the radio core through the knot at 0.″7, as shown in both panels of Figure 1. Figure 3(a) of Yang et al. (2008) indicates that the radio jet changes direction about 2.″6 from the quasar, bending toward the lobe and hotspot at position angle 254°, but we do not have sufficient signal to investigate this in X-rays. We therefore ended the jet box at this distance. We take a width of 1.″5, which is the fit of the FWHM to the 6900 counts in the readout streak at position angles 147° and 327° of the simulated image. The X-ray image contains nine counts in this region, while the simulated X-ray image gives 1100 counts in this box. We scale the latter number by the ratio of 264 counts in the quasar circle to 118472 counts in the same circle of the simulated image, predicting that 2.45 ± 0.17 counts from the quasar will scatter into the region taken for the jet. Taking 2σ above the predicted counts, and an additional 0.082 counts from the background, Poisson statistics gives a probability of 0.29% for the null hypothesis of zero

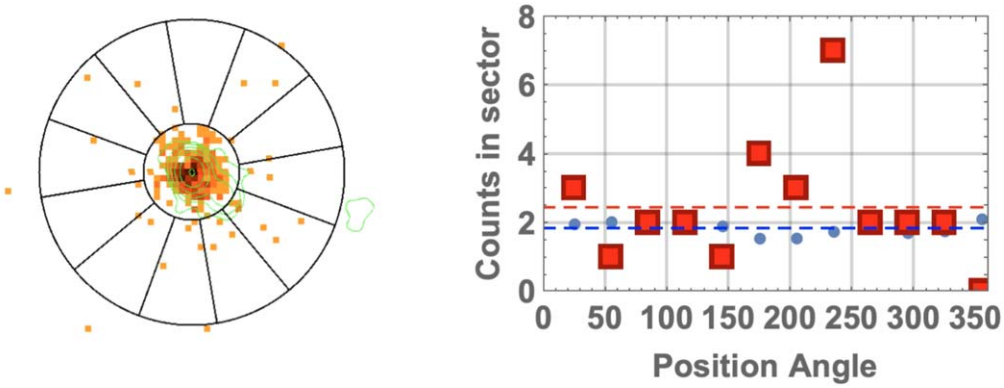

Figure 2. Left: the J1405 X-ray data showing twelve 30° sectors emphasizing the excess X-ray counts from Figure 1 in the direction of the radio extension. The annulus is 0.″95–3″ from the X-ray core, i.e., identical to the length of the jet box in Figure 1. Right: counts per 30° sector in the annulus as a function of position angle measured counterclockwise from North. Blue dots are from the SAOTrace/Marx simulation scaled to the number of counts from the quasar. Red squares are the data. Counts in the sector at 235° are significantly above the average (dashed lines). The readout streak would occur at position angles 147° and 327° and is undetectable due to the low count rate of the quasar and the short exposure time.

extended X-ray emission. Assuming the same spectrum as the quasar, the net jet flux would be 1.0×10^{-14} erg cm^{-2} s^{-1} with an uncertainty of a factor of 2. The rest-frame 2.1–29.4 keV luminosity, if the radiation were unbeamed and isotropic, would be 9×10^{44} erg s^{-1}. (If we had started the jet box 1.″1 from the quasar, we would have had only seven photons, but a lower background of 2.22 counts, and the null hypothesis probability would increase to 0.8%.)

The significance of the extended X-rays can also be assessed by the azimuthal distribution of counts. Figure 2 divides the X-ray image into an annulus from 0.″95 to 3″ and into 30° sectors, centering one sector on the position angle 235° defined by the direction to the knot at 0.″7. The right panel of Figure 2 plots the counts in each sector of the annulus. The average of the data in the 12 sectors is 2.41 counts per sector, and the probability of getting seven counts in the sector with the radio knot by chance is only 1.2%. This calculation gives a higher chance probability of a spurious result because the sector shape is narrower than the Chandra telescope resolution and does not capture all the jet counts. Based on the simulated data, the average counts per sector is only 1.85, and the probability of observing seven counts in the sector with the radio knot would be 0.30%.

The rectangular region used to assess the extended X-ray emission contains a 6.2 GHz flux density of 2.4 mJy from the knot at 0.″7 and its extension. We use that flux density in computing the lower limit X-ray to radio emission ratio. Beyond those radio contours and within the remainder of the X-ray jet region in Figure 1 we derive an upper limit by computing the rms Jy beam^{-1} for the 0.″06 × 0.″06 pixels. This gives 0.134 mJy beam^{-1}. Multiplying by three times the square root of the number of beam areas in the rectangle gives an upper limit of 1.3 mJy for the 6.2 GHz radio emission in the region beyond the radio contours. Our measured flux densities for the core, knot at 0.″7 distance, and lobe at 3.″3 distance are 650 mJy, 25.5 mJy, and 1.7 mJy, respectively. These fall within the error bars of the measurements shown in Figure 5 of Yang et al. (2008).

3.2. J1610+1811

TXS 1607+183 was discovered with a 365 MHz flux density of 415 mJy (Douglas et al. 1980, 1996) in the Texas Survey, and in the MIT Green Bank survey with a flux density

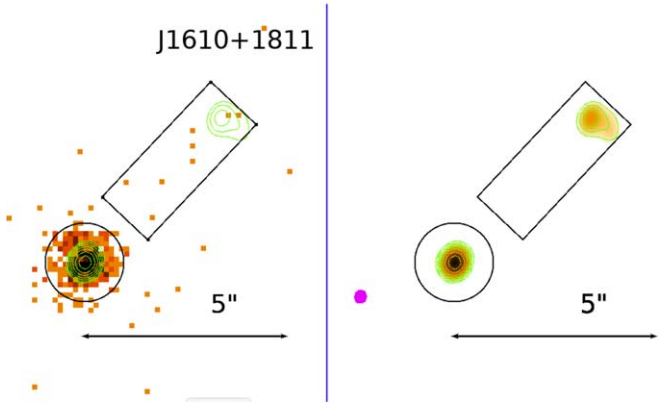

Figure 3. Quasar J1610. Left panel: our 0.5–7 keV Chandra X-ray data binned in 0.″123 pixels. Maximum counts are 13 per pixel. The 0.″95 radius circle centered on the quasar contains 370 photons. The 3.″8 × 1.″5 rectangular region taken for the jet parallels the line from the quasar to the hotspot in the radio image. Right panel: our 6.2 GHz VLA image. Radio contours are shown in both panels, and increase from 0.5 mJy beam^{-1} by factors of 2, with a peak flux density of 66.3 mJy beam^{-1} at the quasar. The restoring beam of 0.″17 × 0.″15 at position angle 343.°45 is shown in magenta.

of 165 mJy at 4.8 GHz (Bennett et al. 1986). The spectral index $\alpha = 0.37$ between those two frequencies classified the object as a flat spectrum radio quasar. Osmer et al. (1994) reported a redshift $z = 3.118$. The ROSAT all sky survey faint source catalog (Voges et al. 2000) lists this quasar with 0.0162 ± 0.0072 counts s^{-1} from 0.1 to 2.4 keV. That rate would correspond to a flux of $(4.4 \pm 2) \times 10^{-13}$ erg cm^{-2} s^{-1} from 0.5 to 7 keV according to the WebPIMMS[11] (Mukai 1993) count rate converter.

We shifted the Chandra image by 0.″28 so that the quasar centroid coincided with the radio position at $16^{h}10^{m}05^{s}.29$ $+18°11'43.''4$. Figure 3 shows our 0.5–7.0 keV and 6.2 GHz images of J1610. In the radio image, a 4.″76 long line from the quasar position to the center of a radio hotspot defines the direction of an expected jet at 317° position angle. Bourda et al. (2010) find a 2 mas long VLBI jet at essentially the same position angle, 316°. Excluding the core and the lobe, we measure a 3σ limit of about 0.34 mJy to the total 6.2 GHz flux

[11] https://heasarc.gsfc.nasa.gov/cgi-bin/Tools/w3pimms/w3pimms.pl

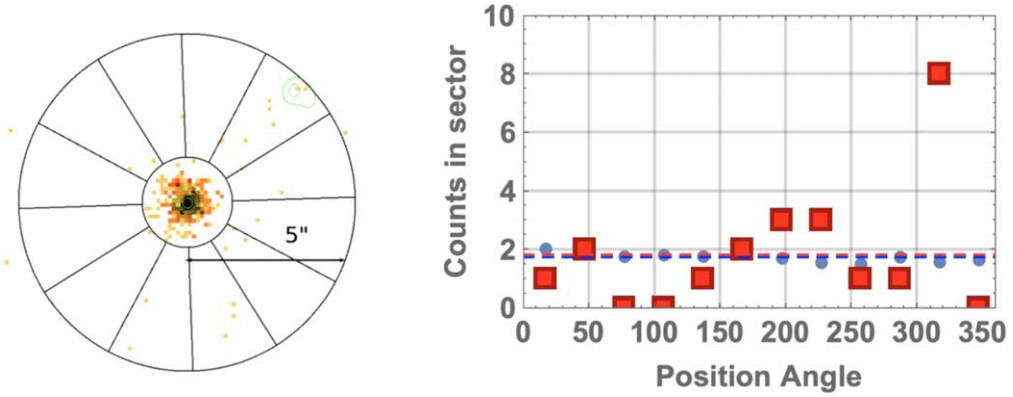

Figure 4. Left: the contours present our 6.2 GHz measurements of J1610. The sectors emphasize the excess X-ray counts from Figure 3 in the direction of the radio extension. The annulus is 1.″4–5.″2 from the X-ray core, i.e., identical to the length of the jet box in Figure 3. Right: counts between 1.″4 and 5.″2 from the quasar, per 30° sector vs. position angle measured counter-clockwise from North. Blue dots are from the SAOTrace/Marx simulation scaled to the number of counts from the quasar. Red squares are the data. The eight counts in the sector at 317° are significantly above the average (dashed lines) of 1.83 counts per sector. The readout streak would occur at position angles 0.°2 and 180.°2 and is undetectable due to the relatively low count rate of the quasar and the short observation time.

density in the region between. We measure $S_{6.2} = 67$ mJy for the quasar core, and $S_{6.2} = 7.6$ mJy from the NW lobe.

We fit the 370 X-ray counts inside a 0.″95 circle about the quasar to a power law with fixed Galactic column density of 3.73×10^{20} H-atoms cm^{-2}. The maximum likelihood Cash statistic gives a best-fit spectral index $\alpha = 0.61 \pm 0.10$. The measured 0.5–7.0 keV flux of $(5.8 \pm 0.5) \times 10^{-13}$ erg cm^{-2} s^{-1} corrected for Galactic absorption implies a rest-frame luminosity of $(5.5 \pm 0.5) \times 10^{46}$ erg s^{-1} in the 2.1–28.8 keV band.

The quasar X-ray core of J1610 is 40% brighter than that of J1405. This prevents testing for a jet at the same 0.″95 distance from the quasar because of the higher density of scattered X-rays. Figure 3 (left panel) shows a region 3.″8 long and 1.″5 wide along the position angle to the radio hotspot and displaced 1.″3 from the quasar. There are eight X-ray photons in this region. The simulation of the quasar predicts that 1.88 ± 0.12 counts are expected to be scattered X-rays from the quasar core. Taking 2σ above the expected scattered counts and adding the detector background of 0.11 counts, the chance of observing eight under the null hypothesis of no extended X-ray emission is 0.22%. If we shrink the X-ray jet region to exclude the radio lobe, there are six X-ray photons, and a 1.6% probability that there is no extended emission. Sector analyses similar to that done for J1405 were carried out. The result using the full X-ray region indicated in Figure 3 is shown in Figure 4, and gives a 0.06% probability that there is no X-ray extension. A sector analysis extending only to 4.″5 from the quasar to exclude the radio lobe, gives a 0.6% probability for observing the 6 counts when expecting 1.53 counts per sector, the average of all twelve sectors. Assuming the same spectrum as the quasar, the six net counts in the jet convert to a flux of 0.9×10^{-14} erg cm^{-2} s^{-1} and a rest-frame 2.1–28.8 keV luminosity of 9×10^{44} erg s^{-1}, if isotropic and without relativistic beaming. The uncertainties are a factor of 2.

4. The X-Ray Dominated Jets

The IC/CMB mechanism offers the simplest model of the jet if the broad-band emission is attributed to a single spectrum of relativistic electrons (e.g., Tavecchio et al. 2000; Celotti et al. 2001; Sambruna et al. 2002, 2004, 2006; Siemiginowska et al. 2002; Marshall et al. 2005, 2011, 2018; Schwartz 2005; Schwartz et al. 2006a, 2006b; Worrall 2009; Massaro et al. 2011; Perlman et al. 2011). For the low redshift, $z \leqslant 2.1$, jets modeled in those references it is also required that there is bulk relativistic motion with Lorentz factor $\Gamma \geqslant 3$ with respect to the co-moving frame of the parent quasar. Bulk relativistic motion is generally inferred for powerful, one-sided quasar jets.

However, there is clear evidence for multiple non-thermal electron populations in jets with complex X-ray morphology, e.g., in 3C 273 (Jester et al. 2006) at $z = 0.158$, PKS 1127-145 at $z = 1.1$ (Siemiginowska et al. 2007), and PKS 0637-752 (Meyer et al. 2015) at $z = 0.653$. Upper limits on the 0.1–100 GeV γ-rays from Fermi observations have been used to argue that IC/CMB cannot give rise to X-ray emission in the jet of PKS 0637-752 (Meyer et al. 2017) and four other jets (Breiding et al. 2017) at redshifts 0.48–1.045, including one that had been modeled as IC/CMB. Nonetheless, at redshifts >3, IC/CMB will be the predominant loss mechanism whenever the magnetic field strength is less than 52 Γ μG, where Γ is the bulk Lorentz factor of the jet, since the energy density of the CMB at redshift z is equivalent to a magnetic field of $3.24(1 + z)^2$ μG. McKeough et al. (2016) noticed a possible increase in the X-ray to radio energy flux ratio at $z > 3$ in a very small sample of X-ray jets. The increasing dominance of IC/CMB at large redshifts has been noted for the limits it may impose on the sizes and ages of FR II radio sources (Scheuer 1977; Blundell et al. 1999). Those limits will affect survey completeness as well as bias correlations of radio source properties (Blundell et al. 1999) and the evolution of black hole activity with redshift (Simionescu et al. 2016). X-ray searches for bright jets which are faint in radio are important to assess the extent of such biases.

There are some interesting similarities and differences among J0730+4049, the first X-ray jet discovered without a radio jet at 1.4 GHz (Simionescu et al. 2016), the two quasars presented here, and the two other, previously observed, quasars in our defined sample. Observed properties are summarized in Table 1. Data for J0730 are from Simionescu et al. (2016), for J1430 from Cheung et al. (2012), and for J1510 from Siemiginowska et al. (2003), Cheung (2004), and Cheung et al. (2005). Data for J1405 and J1610 are from this paper.

Surface brightness is calculated arbitrarily assuming a 0.″5 width, approximately 4 kpc, for each jet. The 0.″5 is the nominal FWHM of the Chandra telescope resolution and comparable to numbers found in the jet of PKS J1421-0643 at $z = 3.69$ (Worrall et al. 2020). The roughly similar surface

Table 1
Comparison of High-redshift X-Ray Jets

Name	Redshift	BH Mass[a] ($10^9 M_\odot$)	Live Time (ks)	Net Jet Counts (0.5–7.0 keV)	X-ray Jet Flux[b]	X-ray Jet Length (arcsec)	X-ray Jet Surface Brightness[b]	X-ray/Radio Ratio[c]	X-ray Jet/Quasar Ratio[d]
J0730+4049	2.50	0.23	19.0	38	2.7	12	0.45	>73	0.18
J1405+0415	3.208	0.87	9.6	6.5	1.0	2	1.0	>12	0.025
J1430+4204	4.72	1[e]	10.6	20.3	1.3	3	0.9	205	0.009
J1510+5702	4.30	0.32	89	123.5	0.76	3	0.5	285	0.03
J1610+1811	3.118	10	9.1	6	0.9	3.8	0.5	>4	0.016

Notes.
[a] Shen et al. (2011).
[b] Flux (10^{-14} erg cm^{-2} s^{-1}) and surface brightness (10^{-14} erg cm^{-2} s^{-1} arcsec^{-2}) are from 0.5 to 7 keV.
[c] νF_ν at 1 keV X-ray divided by νF_ν at 6.2 GHz.
[d] Ratio of X-ray counts.
[e] Fabian et al. (1999).

brightness of these objects is consistent with the expectation from the IC/CMB scenario (Schwartz 2002). While the J0730 jet is similar in surface brightness to the others, the J0730 quasar is an order of magnitude less luminous than the others in this table, and also less than those in Table 6 of Worrall et al. (2020). J1405 and J1610, as well as J1430+4204 and J1510 +5702, have nearly the median 2% jet/core ratio in X-rays found by Marshall et al. (2018). The latter comparison is surprising. A higher ratio would be expected if all low redshift jets were dominated by IC/CMB, but the present result is consistent with the conclusion of Marshall et al. (2011) that the X-ray to radio flux density ratio does not follow the expected $(1+z)^4$ dependence. However, with the expectation that X-ray jets at $z > 3$ are due to IC/CMB, the similarity of the jet/core X-ray ratios to the objects in the Marshall et al. (2018) survey is unexplained. It could be that the quasar core X-ray emission is also dominated by a beamed component as suggested by Worrall et al. (1987). Note that if these jets are beamed in our direction at less than a 10° angle, then at least the innermost 42 kpc of the jet will appear as part of the X-ray core. If the quasar core X-rays are isotropic, a lower jet-to-core ratio may be due to larger angles to our line of sight. Deeper radio observations and longer Chandra observations are necessary to reveal the spectrum and spatial structure of the extended X-ray and radio emission of these systems as well as to understand the emission mechanism and relation to the supermassive black hole powering the quasar.

D.A.S., A.S., and B.S. acknowledge support of NASA contract NAS8-03060 to SAO, and grant GO8-19077X from the CXC. Work by C.C.C. at the Naval Research Laboratory is supported by NASA DPR S-15633-Y. This research made use of the NASA Astrophysics Data System and the NASA/IPAC Extragalactic Database (NED), which is operated by the Jet Propulsion Laboratory, California Institute of Technology, under contract with the National Aeronautics and Space Administration. The National Radio Astronomy Observatory is a facility of the National Science Foundation operated under cooperative agreement by Associated Universities, Inc. D.A.S. thanks Daniel Reese for a script used to generate the quasar simulations.

Facilities: Chandra(ACIS), VLA.

Software: ciao-4.12, SAOTrace-2.0.4_03, Marx-5.5.0, PIMMS v4.11, CASA 4.7.1-REL (r39339).

ORCID iDs

D. A. Schwartz https://orcid.org/0000-0001-8252-4753
A. Siemiginowska https://orcid.org/0000-0002-0905-7375
B. Snios https://orcid.org/0000-0002-4900-928X
D. M. Worrall https://orcid.org/0000-0002-1516-0336
M. Birkinshaw https://orcid.org/0000-0002-1858-277X
C. C. Cheung https://orcid.org/0000-0002-4377-0174
H. Marshall https://orcid.org/0000-0002-6492-1293
G. Migliori https://orcid.org/0000-0003-0216-8053
J. F. C. Wardle https://orcid.org/0000-0002-8960-2942

References

Abazajian, K., Adelman-McCarthy, J. K., Agüeros, M. A., et al. 2003, AJ, 126, 2081
Barthel, P. D., Tytler, D. R., & Thomson, B. 1990, A&AS, 82, 339
Becker, R. H., White, R. L., & Helfand, D. J. 1995, ApJ, 450, 559
Bennett, C. L., Lawrence, C. R., Burke, B. F., et al. 1986, ApJS, 61, 1
Birzan, L., McNamara, B. R., Nulsen, P. E. J., Carilli, C. L., & Wise, M. W. 2008, ApJ, 686, 859
Blandford, R. D., & Rees, M. J. 1974, MNRAS, 169, 395
Blundell, K. M., Rawlings, S., & Willott, C. J. 1999, AJ, 117, 677
Bourda, G., Charlot, P., Porcas, R. W., et al. 2010, A&A, 520, A113
Bourda, G., Collioud, A., Charlot, P., et al. 2011, A&A, 526, A102
Breiding, P., Meyer, E. T., Georganopoulos, M., et al. 2017, ApJ, 849, 95
Bridle, A. H., Hough, D. H., Lonsdale, C. J., et al. 1994, AJ, 108, 766
Bridle, A. H., & Perley, R. A. 1984, ARA&A, 22, 319
Brinkmann, W., Yuan, W., & Siebert, J. 1997, A&A, 319, 413
Cavagnolo, K. W., McNamara, B. R., Nulsen, P. E. J., et al. 2010, ApJ, 720, 1066
Celotti, A., Ghisellini, G., & Chiaberge, M. 2001, MNRAS, 321, L1
Cheung, C. C. 2004, ApJL, 600, L23
Cheung, C. C., Stawarz, Ł., Siemiginowska, A., et al. 2012, ApJL, 756, L20
Cheung, C. C., Wardle, J. F. C., & Lee, N. P. 2005, in 22nd Texas Symp. on Relativistic Astrophysics, ed. P. Chen et al. (Palo Alto, CA: SLAC), 480
Condon, J. J., Hicks, P. D., & Jauncey, D. L. 1977, AJ, 82, 692
Curtis, H. D. 1918, PLicO, 13, 11
Daly, R. A., Sprinkle, T. B., O'Dea, C. P., Kharb, P., & Baum, S. A. 2012, MNRAS, 423, 2498
Davis, J. E., Bautz, M. W., Dewey, D., et al. 2012, Proc. SPIE, 8443, 84431A
Douglas, J. N., Bash, F. N., Bozyan, F. A., et al. 1996, AJ, 111, 1945
Douglas, J. N., Bash, F. N., Torrence, G. W., et al. 1980, PAUTx, 17, 1
Fabian, A. C. 2012, ARA&A, 50, 455
Fabian, A. C., Celotti, A., Pooley, G., et al. 1999, MNRAS, 308, L6
Fabian, A. C., Sanders, J. S., Ettori, S., et al. 2000, MNRAS, 318, L65
Freeman, P., Doe, S., & Siemiginowska, A. 2001, Proc. SPIE, 4477, 76
Fruscione, A., McDowell, J. C., Allen, G. E., et al. 2006, Proc. SPIE, 6270, 62701V
Gobeille, D. B., Wardle, J. F. C., & Cheung, C. C. 2014, arXiv:1406.4797
Gobeille, D. B. P. 2011, PhD thesis, Brandeis Univ.
Gurvits, L. I., Kardashev, N. S., Popov, M. V., et al. 1992, A&A, 260, 82

Hardcastle, M. J., & Croston, J. H. 2020, NewAR, 88, 101539
Harris, D. E., & Krawczynski, H. 2006, ARA&A, 44, 463
Jester, S., Harris, D. E., Marshall, H. L., & Meisenheimer, K. 2006, ApJ, 648, 900
Longair, M. S., Ryle, M., & Scheuer, P. A. G. 1973, MNRAS, 164, 243
Marshall, H. L., Gelbord, J. M., Schwartz, D. A., et al. 2011, ApJS, 193, 15
Marshall, H. L., Gelbord, J. M., Worrall, D. M., et al. 2018, ApJ, 856, 66
Marshall, H. L., Schwartz, D. A., Lovell, J. E. J., et al. 2005, ApJS, 156, 13
Massaro, F., Harris, D. E., & Cheung, C. C. 2011, ApJS, 197, 24
McKeough, K., Siemiginowska, A., Cheung, C. C., et al. 2016, ApJ, 833, 123
Meyer, E. T., Breiding, P., Georganopoulos, M., et al. 2017, ApJL, 835, L35
Meyer, E. T., Georganopoulos, M., Sparks, W. B., et al. 2015, ApJ, 805, 154
Mukai, K. 1993, Legacy, 3, 21, https://heasarc.gsfc.nasa.gov/docs/journal/pimms3.html
O'Dea, C. P., Daly, R. A., Kharb, P., Freeman, K. A., & Baum, S. A. 2009, A&A, 494, 471
Osmer, P. S., Porter, A. C., & Green, R. F. 1994, ApJ, 436, 678
Perley, R. A., Willis, A. G., & Scott, J. S. 1979, Natur, 281, 437
Perlman, E. S., Georganopoulos, M., Marshall, H. L., et al. 2011, ApJ, 739, 65
Peterson, B. A., Jauncey, D. L., Wright, A. E., et al. 1978, ApJL, 222, L81
Planck Collaboration, Ade, P. A. R., Aghanim, N., et al. 2016, A&A, 594, A13
Rawlings, S., & Saunders, R. 1991, Natur, 349, 138
Readhead, A. C. S., Cohen, M. H., & Blandford, R. D. 1978, Natur, 272, 131
Rees, M. J. 1971, Natur, 229, 312
Sambruna, R. M., Gambill, J. K., Maraschi, L., et al. 2004, ApJ, 608, 698
Sambruna, R. M., Gliozzi, M., Donato, D., et al. 2006, ApJ, 641, 717
Sambruna, R. M., Maraschi, L., Tavecchio, F., et al. 2002, ApJ, 571, 20
Scheuer, P. A. G. 1974, MNRAS, 166, 513
Scheuer, P. A. G. 1977, Radio Astronomy and Cosmology (Dordrecht: D. Reidel), 343
Schwartz, D. 2010, PNAS, 107, 7190
Schwartz, D., Siemiginowska, A., Worrall, D., et al. 2019, AN, 340, 30
Schwartz, D. A. 2002, ApJL, 569, L23
Schwartz, D. A. 2005, in 22nd Texas Symp. on Relativistic Astrophysics, ed. P. Chen et al. (Palo Alto, CA: SLAC), 38
Schwartz, D. A., Marshall, H. L., Lovell, J. E. J., et al. 2006a, ApJ, 640, 592
Schwartz, D. A., Marshall, H. L., Lovell, J. E. J., et al. 2006b, ApJL, 647, L107
Shen, Y., Richards, G. T., Strauss, M. A., et al. 2011, ApJS, 194, 45
Shimmins, A. J., Bolton, J. G., & Wall, J. V. 1975, AuJPA, 34, 63
Siemiginowska, A, Bechtold, J., Aldcroft, T. L., et al. 2002, ApJ, 570, 543
Siemiginowska, A., Stawarz, Ł., Cheung, C. C., et al. 2007, ApJ, 657, 145
Siemiginowska, A., Smith, R. K., Aldcroft, T. L., et al. 2003, ApJL, 598, L15
Simionescu, A., Stawarz, Ł., Ichinohe, Y., et al. 2016, ApJL, 816, L15
Tavecchio, F., Maraschi, L., Sambruna, R. M., & Urry, C. M. 2000, ApJL, 544, L23
Turland, B. D. 1975, MNRAS, 172, 181
Voges, W., Aschenbach, B., Boller, T., et al. 2000, IAUC, 7432, 3
Waggett, P. C., Warner, P. J., & Baldwin, J. E. 1977, MNRAS, 181, 465
Willott, C. J., Rawlings, S., Blundell, K. M., & Lacy, M. 1999, MNRAS, 309, 1017
Worrall, D. M. 2009, A&ARv, 17, 1
Worrall, D. M., Birkinshaw, M., Marshall, H. L., et al. 2020, MNRAS, 497, 988
Worrall, D. M., Giommi, P., Tananbaum, H., et al. 1987, ApJ, 313, 596
Yang, J., Gurvits, L. I., Lobanov, A. P., et al. 2008, A&A, 489, 517
Yuan, W., Fabian, A. C., Celotti, A., et al. 2003, MNRAS, 346, L7
Zamorani, G., Henry, J. P., Maccacaro, T., et al. 1981, ApJ, 245, 357